Ultrasonics Sonochemistry 89 (2022) 106114

Contents lists available at ScienceDirect

Ultrasonics Sonochemistry

journal homepage: www.elsevier.com/locate/ultson

Sonochemical synthesis of supersaturated Ga–Al liquid-alloy fine particles and Al^{3+}-doped γ-Ga_2O_3 nanoparticles by direct oxidation at near room temperature

Toshiki Yamanaka, Yamato Hayashi *, Hirotsugu Takizawa

Graduate School of Engineering, Department of Applied Chemistry, Tohoku University, 6-6 Aoba, Aramaki, Aobaku, Sendai 980-8579, Japan

ARTICLE INFO

Keywords:
Supersaturation
Liquid alloy
Nanoparticles
Ultrasound
Room temperature
Direct oxidation

ABSTRACT

In this study, we investigated the fabrication of supersaturated gallium (Ga)–aluminum (Al) liquid alloy and Al^{3+}-doped γ-Ga_2O_3 nanoparticles (NPs) at near room temperature (60 °C) using sonochemical and sonophysical effects. Supersaturated Ga–Al liquid alloy microparticles (D_{av} = 1.72 μm) were formed and stabilized at 60 °C by the thermal nonequilibrium field provided by sonochemical hot spots. Compared with liquid Ga, supersaturated Ga–Al liquid alloy was rapidly oxidized to a uniform oxide without Al_2O_3 or Al deposition. Thus, ultrafine Al^{3+}-doped γ-Ga_2O_3 NPs were obtained after only 1 h of ultrasonic irradiation at 60 °C. The oxidation of liquid Ga was remarkably accelerated by alloying with metallic Al and ultrasonic irradiation, and the time was shortened. The average diameter and surface area of the γ-Ga_2O_3-based NPs were 59 nm and 181 m^2/g, respectively. Compared with γ-Ga_2O_3, the optical bandgap of the Al^{3+}-doped γ-Ga_2O_3 NPs was broadened, and the thermal stability improved, indicating Al^{3+}-doping into the γ-Ga_2O_3 lattice. However, the lattice constant of γ-Ga_2O_3 was almost unchanged with or without Al^{3+}-doping. Al^{3+} was introduced into the defect sites of Ga^{3+}, which were massively induced in the defective spinel structure during ultrasonic processing. Therefore, sonochemical processing, which provides nonequilibrium reaction fields, is suitable for the synthesis of supersaturated and metastable materials in metals and ceramics fields.

1. Introduction

Gallium oxide (Ga_2O_3) is a wide-bandgap semiconductor with five polymorphs (α, β, γ, ε, and δ). β-Ga_2O_3 has attracted attention as a next-generation power semiconductor, and the synthesis and properties of β-Ga_2O_3 have been extensively investigated [1–4]. Compared with β-Ga_2O_3, only a few studies on the other polymorphs of Ga_2O_3 have been reported. There is a need for further studies on Ga_2O_3 polymorphs to clarify their properties. Previous studies have revealed that γ-Ga_2O_3, which has a defective spinel structure, exhibits high photocatalytic activity, denitrification activity, and phosphor properties [5–7]. However, γ-Ga_2O_3 has been synthesized using limited homogeneous aqueous solution methods, such as hydrothermal, solvothermal, and sol–gel methods, because γ-Ga_2O_3 transforms to β-Ga_2O_3 at approximately 600 °C. Metal salts, which can dissolve in solvents, such as water and alcohol, are generally used as raw materials in homogeneous aqueous solution methods. In such liquid processes, counter anions ($(NO_3)_3^-$, SO_4^{2-}, Cl^-, etc.) remaining in the solution must be removed after the reactions. Furthermore, harsh reaction conditions, such as high temperature and pressure, are required for liquid-state reaction processes. Thus, there is a need for better methods for synthesizing γ-Ga_2O_3 and other ceramics materials without thermal treatment and waste liquid emission.

Recently, ultrasonic processing has attracted attention as a sustainable material processing technique. The synthesis of inorganic materials via ultrasonic processing has been investigated, and various metal nanoparticles (NPs), including Ga NPs, have been synthesized using ultrasound [8–15]. The synthesis of Ga NPs using various solvents has also been investigated because nanosized droplets of Ga can be synthesized in immiscible solvents using ultrasound owing to the low melting point of Ga (T_m = 29.8 °C). Kumar reported that Ga NPs (0.2–5 μm) can be synthesized via ultrasonic irradiation of hexane and dodecane solvents [16]. In addition, they synthesized gallium oxyhydroxide (GaOOH) via the ultrasonic irradiation of Ga in water [17]. Based on the above processes, NPs of metals or hydroxides can be synthesized using only ultrasound.

* Corresponding author.
E-mail address: yamato.hayashi.b6@tohoku.ac.jp (Y. Hayashi).

https://doi.org/10.1016/j.ultsonch.2022.106114
Received 28 June 2022; Received in revised form 1 August 2022; Accepted 4 August 2022
Available online 9 August 2022
1350-4177/© 2022 The Author(s). Published by Elsevier B.V. This is an open access article under the CC BY-NC-ND license (http://creativecommons.org/licenses/by-nc-nd/4.0/).

Metal NPs have specific properties different from those of bulk materials, including surface plasmon resonance and low-temperature sintering, due to their paucity of atoms in a particle. Metal NPs also exhibit high surface activity. However, the surfaces of metal NPs are easily oxidized because the Gibbs energy of the oxidation reaction of almost all metals is negative. The surface oxidation of metal NPs decreases their conductivity and sinterability, particularly that of basic metal NPs [18,19]. However, considering that the ease of oxidation of metal NPs can facilitate the oxidation of metals, oxide NPs can be synthesized from metal NPs. Takano et al. synthesized γ-Ga_2O_3 fine particles via miniaturization and oxidation processes by ultrasonic irradiation of liquid Ga in hydrazine monohydrate ($N_2H_4{\cdot}H_2O$) at room temperature [20]. Kumar et al. reported that when liquid Ga is sonicated in H_2O, it oxidizes to GaOOH because of the hydroxyl radicals (OH•) generated from H_2O by ultrasound. In contrast, when sonicated in $N_2H_4{\cdot}H_2O$, liquid Ga does not oxidize to GaOOH because the generation of OH• is suppressed by $N_2H_4{\cdot}H_2O$. Liquid Ga is directly oxidized to γ-Ga_2O_3 by reactive oxygen species generated from sonicated $N_2H_4{\cdot}H_2O$, and γ-Ga_2O_3 fine particles can be obtained. Nanosized γ-Ga_2O_3 can be synthesized at room temperature via ultrasonic processing. Using this method, γ-Ga_2O_3-based nanosized materials and other nanoceramic materials can be synthesized at room temperature.

Owing to the low melting point of metallic Ga (T_m = 29.8 °C), liquid Ga-based alloys (Ga–M; M = In, Al, Zn, etc.) can be obtained at low temperatures [21–23]. However, at room temperature, considering energy conservation, only a small atomic percentage of metal (2.1 atom% for Al) can dissolve in liquid Ga at 25 °C. To dissolve excessive Al in liquid Ga, the formation of a supersaturation state is required. However, it is difficult to fabricate supersaturated materials via general material processing techniques using thermodynamic equilibrium fields. To synthesize supersaturated materials, nonequilibrium reaction fields are employed to deviate from the equilibrium law. Suda synthesized a CeO_2–ZrO_2-supersaturated solid solution, a component of a three-way catalyst for purifying gas emitted from gas-powered cars, via high-speed ball milling using CeO_2 powder, ZrO_2 ball, and ethanol (EtOH) [24]. Furthermore, Romankov synthesized an Al-rich supersaturated Ti–Al solid solution by mechanical alloying (high-energy ball impacts) using Ti and Al powders and a Ti substrate [25]. These methods are similar in that localized high-temperature and -pressure fields are formed by colliding particles on very short time scales, which is the same in ultrasonic processing techniques, where local nonequilibrium fields are obtained at room temperature on short time scales. Cavitation generated via ultrasonic processing in the liquid phase repeatedly expands and contracts, then collapses, resulting in an adiabatic compression state inside the cavity. Numerous localized high-temperature and -pressure fields (hot spots) are formed in the liquid phase and are repeatedly generated and extinguished on a microsecond basis under room-temperature conditions. Furthermore, since cavitation collapse is accompanied by physical effects, such as microjet flows and shock waves, extreme reaction fields can be formed by hot spots, microjet flows, and shock waves. Using sonochemical and sonophysical effects to form liquid Ga–M alloys, supersaturated liquid Ga–M alloys, in which metal M is more dissolved in liquid Ga than the theoretical composition of the Ga–M phase diagram, can be obtained.

A few studies on the synthesis of ceramics by oxidation of liquid alloy particles have been reported. The morphology of γ-Ga_2O_3-based particles obtained by oxidizing Ga–M liquid alloys using ultrasound and $N_2H_4{\cdot}H_2O$ is of great interest. The oxidation behavior of Ga–M liquid alloys is expected to differ greatly, depending on M. Nanocomposites (M_xO_y/γ-Ga_2O_3, M/γ-Ga_2O_3, etc.) or metal-doped γ-Ga_2O_3 NPs can easily be obtained at room temperature. This would promote the development of the physical properties of γ-Ga_2O_3. However, γ-Ga_2O_3 has not been successfully synthesized and requires further exploration. There is a need for low-temperature synthesis methods for ceramic nanomaterials.

Metallic Al is homologous with Ga, and its oxide has various crystal polymorphs, similar to Ga_2O_3. In this study, Al was selected as an additive metal to liquid Ga. The preparation of supersaturated liquid Ga–Al alloys and the near-room-temperature synthesis of γ-Ga_2O_3-based nanomaterials via ultrasonic irradiation of Ga–Al liquid alloys were investigated.

2. Experimental

2.1. Materials

Ga (Rasa Industries, Ltd.) and Al (FUJIFILM Wako Pure Chemical Corporation, 99.0 %) were used as starting materials. EtOH (JAPAN ALCOHOL TRADING Co. Ltd., 99.0 %) was used as an organic solvent, which is immiscible with liquid metal. $N_2H_4{\cdot}H_2O$ (FUJIFILM Wako Pure Chemical Corporation 98.0 %) was used as an oxidizing agent for Ga.

2.2. Equipment

Fig. 2 shows a schematic of the experimental setup. A sonoreactor (Honda electronics Co., Ltd.) was used for ultrasonic irradiation. Ultrasound was irradiated to dispersion in a 300-mL Erlenmeyer flask through a water bath.

2.3. Characterization

The crystalline phase and lattice constant of the samples were determined by powder X-ray diffraction (XRD, D2 phaser, Bruker AXS) using Cu kα (λ = 0.154184 nm) radiation. The morphologies of the products were characterized by field-emission scanning electron microscopy (FE-SEM, JSM-7610F, JEOL Ltd.) and field-emission scanning transmission electron microscopy (FE-STEM, HD-2700, Hitachi High-Tech Corp.). The specific surface area (S_{BET}) of the products was measured using a catalyst characterization analyzer (BELCAT II, MicrotracBEL Corp.), and the diffuse reflection spectra were obtained using an ultraviolet–visible near-infrared spectrometer (V-750, JASCO Corp.). The obtained diffuse reflection spectra were converted to absorption spectra using the Kubelka–Munk function. The thermal properties of the sample were measured by thermogravimeter-differential scanning calorimetry (TG-DSC, STA 449 *F1 Jupiter*, NETZSCH).

2.4. Preparation of γ-Ga_2O_3:Al NPs

Fig. 3 shows a flowchart of the experiments. γ-Ga_2O_3-based NPs were synthesized via two-step ultrasonic irradiation. Ga (1 g) and Al (0.05 g) granules were put into a 300-mL Erlenmeyer flask and mixed at 150 °C for 10 min. After Al was dissolved in liquid Ga, the flask was cooled to approximately 60 °C, and EtOH (50 mL) degassed by ultrasound was added. An infinitesimal amount of gas was evolved while EtOH was added. The flask was sonicated (24 kHz, 100 W) for 24 h (i.e., the miniaturization step for the liquid alloy). Afterward, $N_2H_4{\cdot}H_2O$ (50 mL) was added to the flask, and ultrasound (24 kHz, 100 W) was irradiated to the flask for 24 h (the oxidation step for the liquid alloy). The temperature of the dispersion was maintained at approximately 60 °C using a water bath, which was controlled by a circulator (CTP-3000, TOKYO RIKAKIKAI Co., Ltd.). After ultrasonic irradiation, EtOH and $N_2H_4{\cdot}H_2O$ in the dispersion were removed by centrifugation, and the product was dried in air. The dried product was calcined at 400 °C–1000 °C for 3 h to investigate the changes in the absorption and crystalline phase.

3. Results

3.1. Miniaturization of liquid Ga and Ga–Al liquid alloy

Fig. 4 shows the XRD patterns of liquid Ga and Ga–Al liquid alloy sonicated in EtOH. The XRD patterns of both liquid Ga and Ga–Al liquid alloy (Fig. 4(a) and (b), respectively) show no crystalline peaks. The

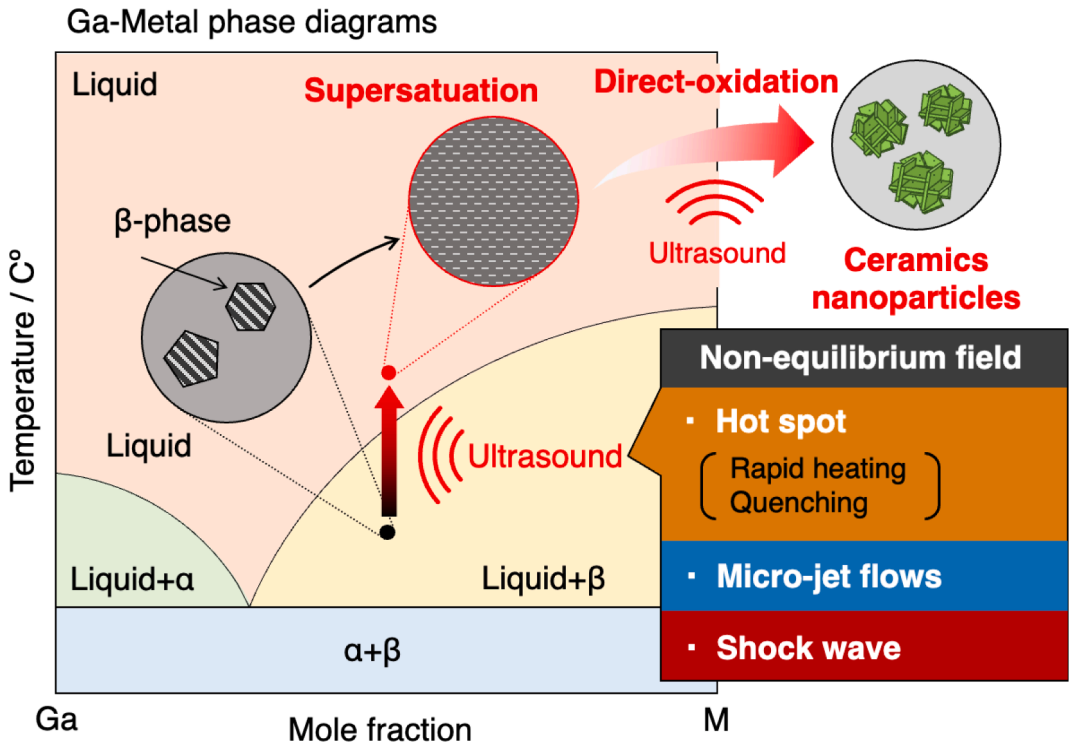

Fig. 1. Schematic of the low-temperature fabrication process for supersaturated liquid alloy and ceramic nanoparticles (NPs) using ultrasound.

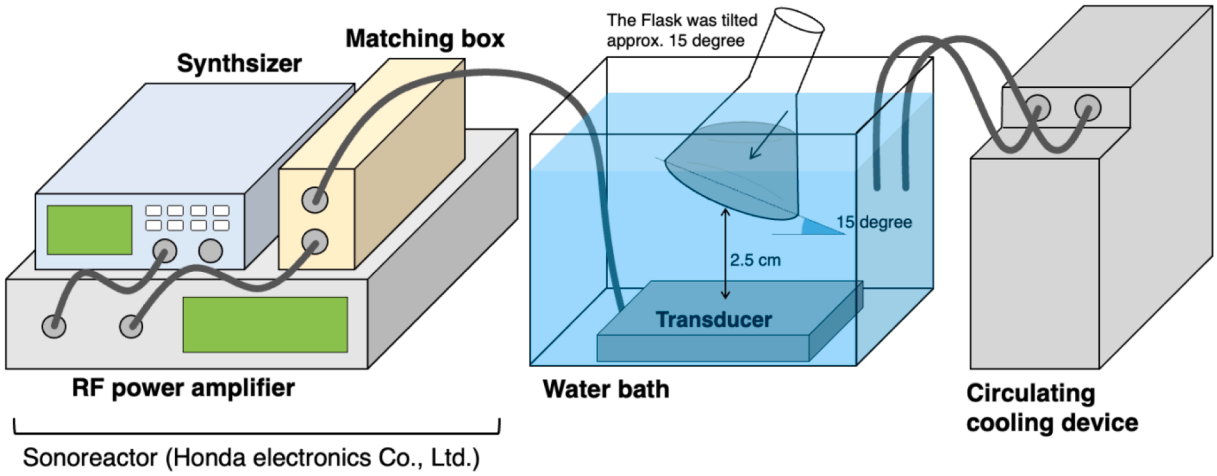

Fig. 2. Schematic of the experimental equipments.

XRD patterns of the liquid alloy show no crystalline peaks attributed to Al, indicating that, with ultrasonic irradiation at 60 °C, the liquid Ga and metallic Al in the flask formed a supersaturated Ga–Al liquid alloy.

Fig. 5 shows FE-SEM images of the liquid Ga and Ga–Al liquid alloy sonicated in EtOH. The diameters of the liquid Ga and Ga–Al liquid alloy particles were reduced by ultrasonic irradiation. Compared with that of Ga particles sonicated for 24 h, the diameter of liquid Ga particles sonicated for 1 h decreased from 1.74 μm to 249 nm, and liquid Ga NPs were obtained. In the case of Ga–Al liquid alloy, the diameter of the liquid Ga–Al particles decreased from 3.48 μm to 1.72 μm after sonication, and liquid Ga–Al alloy microparticles were obtained.

3.2. Oxidation of Ga NPs and Ga–Al microparticles

Fig. 6 shows the XRD patterns of liquid Ga NPs and Ga–Al liquid alloy microparticles sonicated in a mixed solvent of EtOH and $N_2H_4{\cdot}H_2O$. The XRD patterns of liquid Ga sonicated for 6 h show crystalline peaks attributed to γ-Ga_2O_3(PDF: 01–082-3194). The peaks of γ-Ga_2O_3 became sharper with ultrasonic irradiation. The liquid Ga particles were slowly oxidized to γ-Ga_2O_3. However, liquid Ga–Al alloy sonicated for only 1 h showed only sharp diffraction peaks attributed to the spinel structure. This indicates that the Ga–Al liquid alloy was rapidly oxidized to spinel oxide. It is considered Al^{3+}-doped γ-Ga_2O_3 (Ga^{3+}/Al^{3+} = 88:12 [atom %]) NPs were obtained at 60 °C because peaks of Al-containing compounds were not observed.

Fig. 7 shows FE-SEM images of the liquid Ga NPs and Ga–Al alloy microparticles sonicated in a mixed solvent of EtOH and $N_2H_4{\cdot}H_2O$. γ-Ga_2O_3 uniformly nucleated on the Ga NPs, and the nucleus of γ-Ga_2O_3 remarkably increased with ultrasonication. SEM revealed cracks in the γ-Ga_2O_3 particles (as shown Fig. 7B). The average diameter (D_{av}) and specific surface area of the γ-Ga_2O_3 particles after 24-h sonication were 254 nm and 91 m^2/g, respectively. However, in the case of the Ga–Al

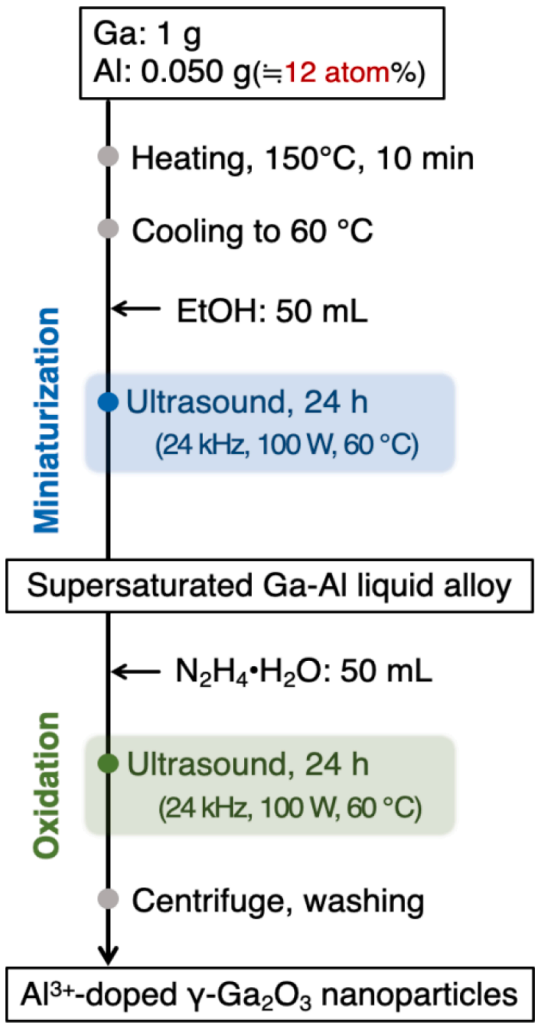

Fig. 3. Flowchart for preparing γ-Ga_2O_3:Al NPs via ultrasonic irradiation.

liquid alloy, edged NPs, which are inferred to be Al^{3+}-doped γ-Ga_2O_3, were obtained after 1-h sonication. The Ga–Al particles were bigger than the Ga particles before oxidation. The crystallinity of the edged NPs increased with sonication. After 24-h sonication, Al^{3+}-doped γ-Ga_2O_3 fine NPs with a specific surface area of 181 m^2/g were obtained.

Fig. 8 shows the TEM images of liquid Ga NPs sonicated in a mixed solvent of EtOH and $N_2H_4{\cdot}H_2O$. When sonicated for 3 h, uniform liquid spherical particles were observed., and the sample sonicated for 6 h yielded γ-Ga_2O_3/liquid Ga core–shell particles. With increased ultrasonic irradiation, γ-Ga_2O_3 crystals grew on the surface of the particles, making them needle-shaped. After 24-h sonication, hollow γ-Ga_2O_3 particles were obtained.

3.3. *Property of γ-Ga_2O_3:Al NPs*

Fig. 9 shows the absorption spectra of γ-Ga_2O_3 and Al^{3+}-doped γ-Ga_2O_3 calcined at 400 °C–800 °C in air. γ-Ga_2O_3 obtained from liquid Ga NPs showed absorption in the range of 300–800 nm and appeared as a gray powder. This indicates the presence of liquid Ga that was not oxidized during the 24-h sonication in the γ-Ga_2O_3. γ-Ga_2O_3 calcined at 800 °C did not show absorption peaks in the visible range, indicating that Ga remaining in the γ-Ga_2O_3 was oxidized to β-Ga_2O_3 during the thermal treatment. The optical bandgap of γ-Ga_2O_3 was reduced after calcination at 400 °C.

In contrast, the Al^{3+}-doped γ-Ga_2O_3 obtained from the Ga–Al liquid alloy did not show absorption peaks in the range of 300–800 nm and appeared as a white powder. This shows that the Ga–Al liquid alloy was completely oxidized to Al^{3+}-doped γ-Ga_2O_3. The oxidation reaction was facilitated by the dissolution of Al in the liquid Ga. The optical bandgap of the sample was also narrowed after calcination at 400 °C in air, similar to the case of γ-Ga_2O_3. Compared with the bandgap of γ-Ga_2O_3, that of Al^{3+}-doped γ-Ga_2O_3 increased regardless of calcination. In the previous studies, the bandgap of γ-Ga_2O_3 was widened by Al^{3+}-doping [26], which is consistent with our results herein.

Fig. 10 shows the DSC curve of γ-Ga_2O_3 and Al^{3+}-doped γ-Ga_2O_3 under a 20-mL/min He flow. γ-Ga_2O_3 obtained from liquid Ga NPs showed endothermic peaks at −17.1 °C and −36.0 °C. Ga NPs showed endothermic peaks in the range from −40 °C to −20 °C [27]. The

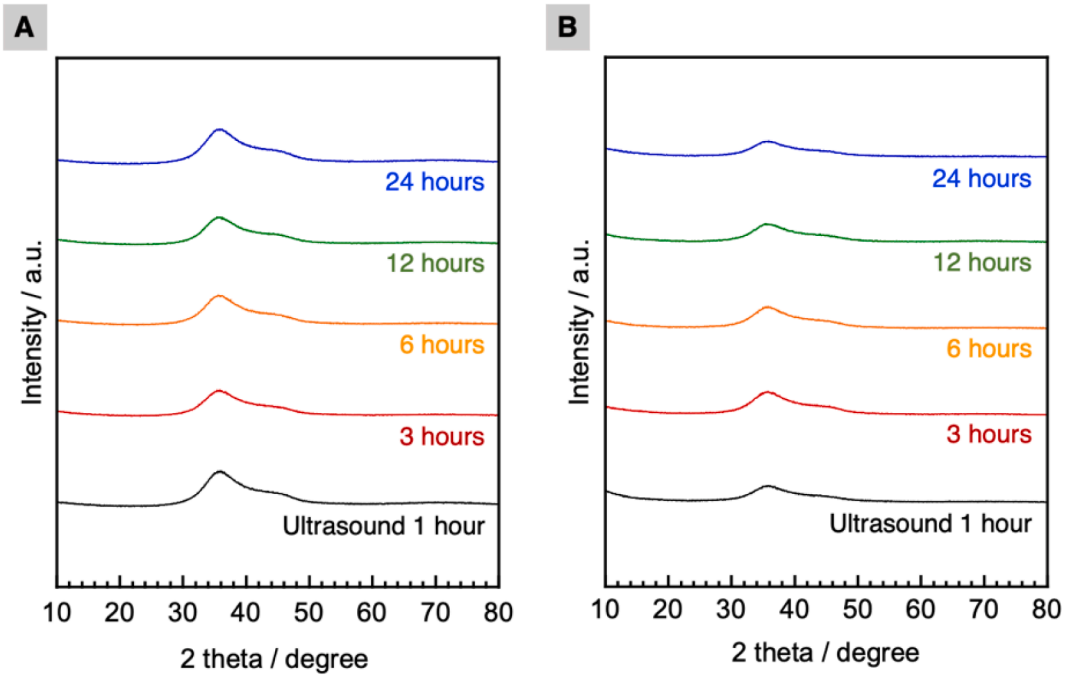

Fig. 4. X-ray diffraction (XRD) patterns of liquid Ga (A) and Ga–Al liquid alloy (B) sonicated in EtOH.

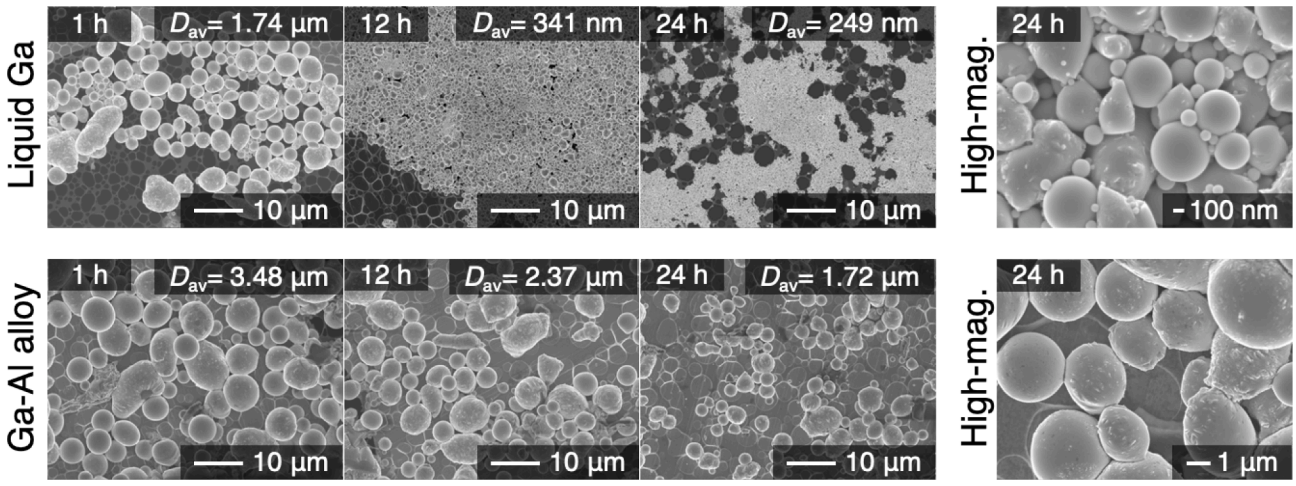

Fig. 5. FE-SEM images of liquid Ga and Ga–Al liquid alloy particles irradiated in EtOH.

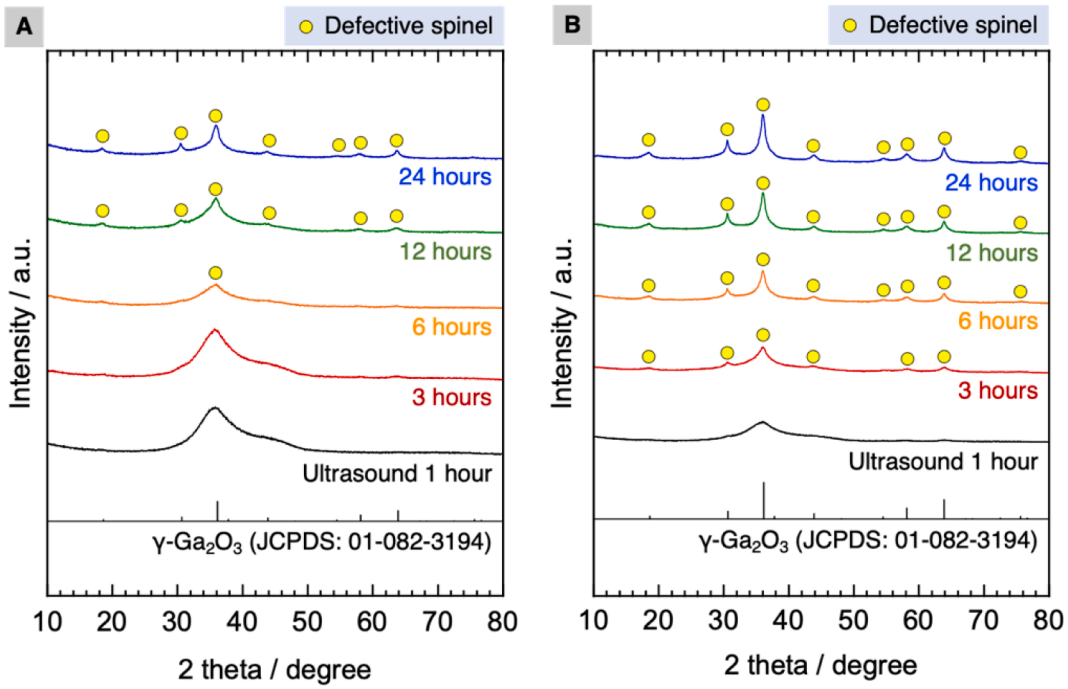

Fig. 6. XRD patterns of liquid Ga and Ga–Al alloy sonicated in ethanol (EtOH) and hydrazine monohydrate ($N_2H_4{\cdot}H_2O$).

γ-Ga_2O_3 obtained herein contains unreacted liquid Ga that was not oxidized. However, the Al^{3+}-doped γ-Ga_2O_3 obtained from the Ga–Al liquid alloy did not show endothermic peaks attributed to metal NPs, indicating that the Ga–Al liquid alloy was completely oxidized to Al^{3+}-doped γ-Ga_2O_3. The DSC curve of γ-Ga_2O_3 shows exothermic peaks at 520.6 °C. The phase-transition temperature was 520 °C. On the other hand, the DSC curve of Al^{3+}-doped γ-Ga_2O_3 showed an exothermic peak at 672.1 °C. Takahashi et al. reported an increase in the phase-transition point of γ-Ga_2O_3 with Al^{3+}-doping [28,29]. In this study, Al^{3+}-doped γ-Ga_2O_3 NPs were obtained via the sonochemical oxidation of Ga–Al liquid alloy.

Fig. 11 shows the XRD patterns of γ-Ga_2O_3 and Al^{3+}-doped γ-Ga_2O_3 calcined at 400 °C–800 °C. Ga_2O_3 completely transformed from the γ-phase (defective spinel) to the β-phase (β-Gallia) dung calcination at 800 °C. Previous studies have shown that the phase-transition temperature of γ-Ga_2O_3 is approximately 550 °C [30], which is consistent with the value obtained herein. However, Al^{3+}-doped γ-Ga_2O_3 did not completely transform to β-phase during calcination at 800 °C. After calcination at 800 °C, Al^{3+}-doped γ-Ga_2O_3 showed a weak diffraction peak of the γ-phase, indicating an increase in the phase-transition point of γ-Ga_2O_3 with Al^{3+}-doping.

Fig. 12 shows the XRD patterns of all products (γ-Ga_2O_3, Al^{3+}-doped γ-Ga_2O_3, β-Ga_2O_3 obtained from the calcination of γ-Ga_2O_3, Al^{3+}-doped β-Ga_2O_3 obtained from the calcination of γ-Ga_2O_3, Al^{3+}-doped γ-Ga_2O_3 at 1000 °C in the air). Compared with those of γ-Ga_2O_3, the degree of diffraction peaks of Al^{3+}-doped γ-Ga_2O_3 did not change with Al^{3+}-doping.

Both γ-Ga_2O_3 and Al^{3+}-doped γ-Ga_2O_3 transformed into the β-phase when calcined at 1000 °C in the air. B-Ga_2O_3 and Al^{3+}-doped β-Ga_2O_3 showed diffraction peaks corresponding to β-Ga_2O_3 (JCPDS:00-041-1103). Compared with those of β-Ga_2O_3, the degree of diffraction peaks of Al^{3+}-doped β-Ga_2O_3 increased. The shift in the peaks of Al^{3+}-doped β-Ga_2O_3 resulted in the shrinking of the unit cell of β-Ga_2O_3 lattice. Considering the ionic radii of Ga^{3+} (0.0620 nm) and Al^{3+} (0.0535 nm) in six-coordination [31], the shrinking of the unit cell is attributed to the substitution of Ga^{3+} with Al^{3+} in the β-Ga_2O_3 lattice (Table 1).

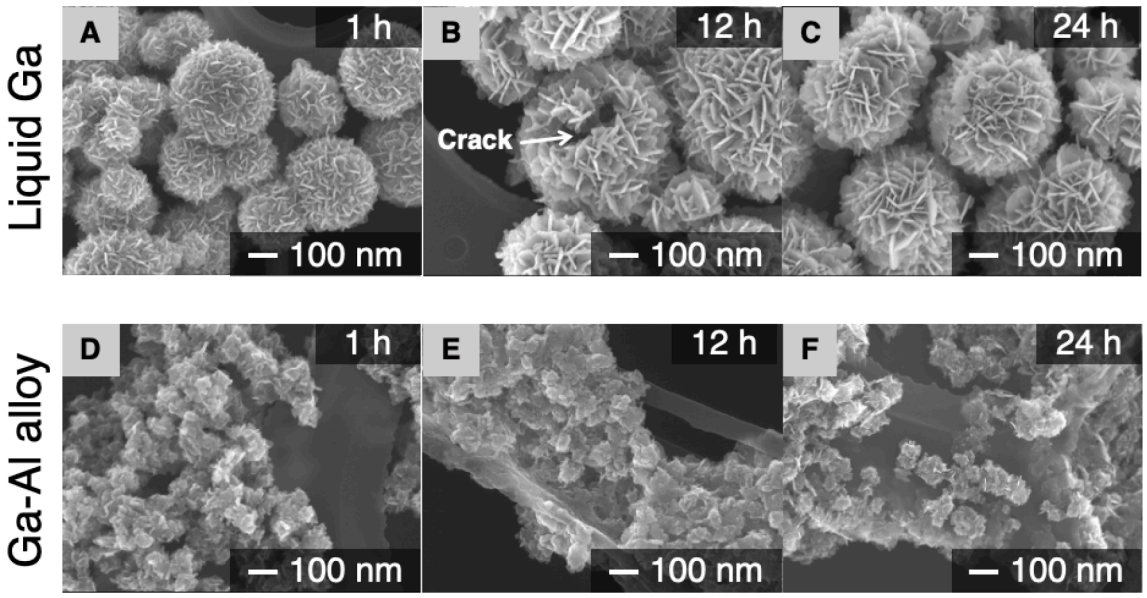

Fig. 7. Field-emmision scanning electron microscopy (FE-SEM) images of liquid Ga NPs and Ga–Al liquid alloy microparticles irradiated in a mixed solvent of EtOH and $N_2H_4{\cdot}H_2O$ (SEM images shows the oxidation behavior of each liquid metal particles).

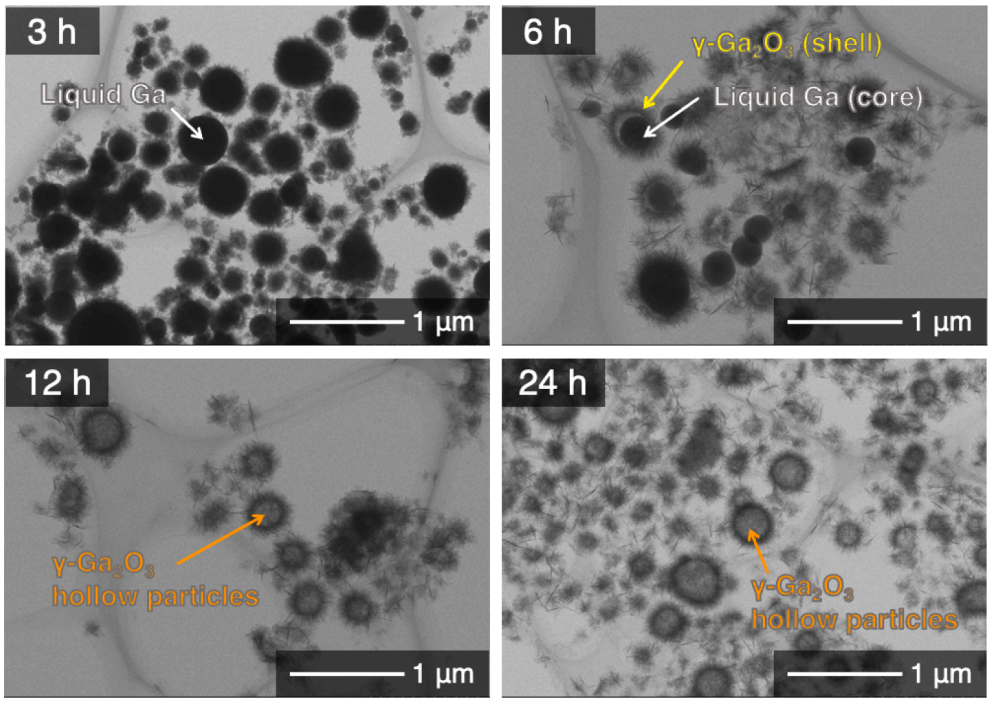

Fig. 8. FE-TEM images of liquid Ga NPs irradiated in a mixed solvent of EtOH and $N_2H_4{\cdot}H_2O$.

Previous studies have reported a decrease in the lattice constant of γ-Ga_2O_3 with Al^{3+}-doping [5,24]. The lattice constant of Al^{3+}-doped γ-Ga_2O_3 remained unchanged, and that of Al^{3+}-doped β-Ga_2O_3 decreased, indicating that Al^{3+} in the Al^{3+}-doped γ-Ga_2O_3 lattice exists on defect sites of a defective spinel structure.

4. Discussion

4.1. Roll of ultrasound irradiation in the miniaturization of liquid Ga and Ga–Al alloy

4.1.1. Ultrasonic irradiation effect on liquid Ga

Fig. 13 shows schematics of the miniaturization mechanisms of liquid Ga (upper) and Ga–Al liquid alloy (lower). Ultrasound irradiation in EtOH refines liquid metal and alloy into NPs. This phenomenon is caused by sonophysial effects, such as the microjet flows and shock waves associated with cavitation collapse [32].

Herein, liquid Ga was refined to NPs by sonophysical effects,

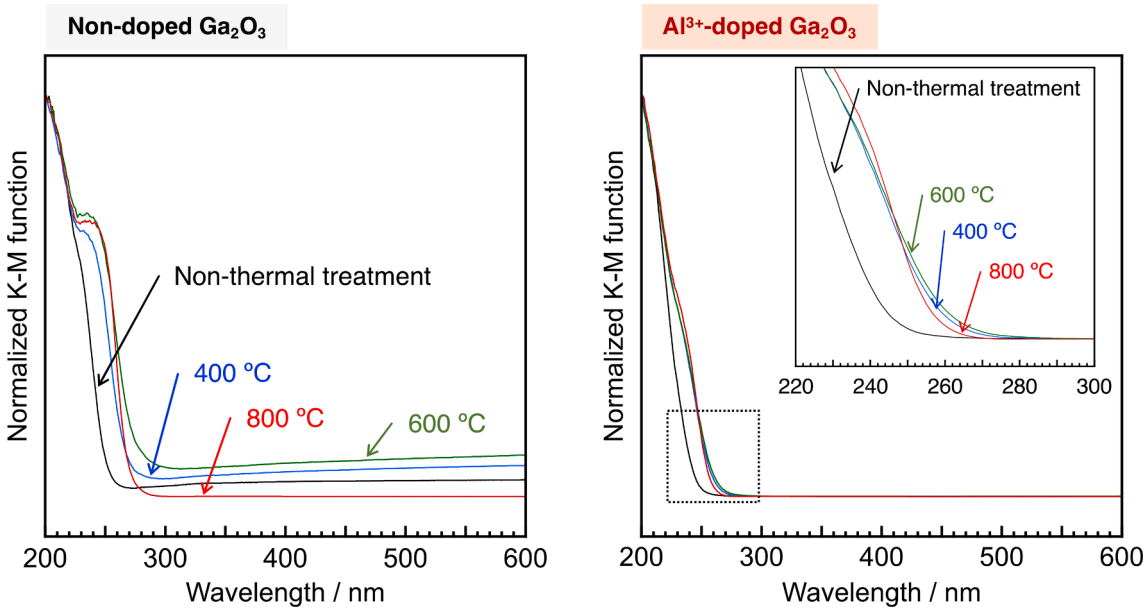

Fig. 9. Ultraviolet–visible (UV–vis) reflection spectra of γ-Ga_2O_3:Al powder after calcination.

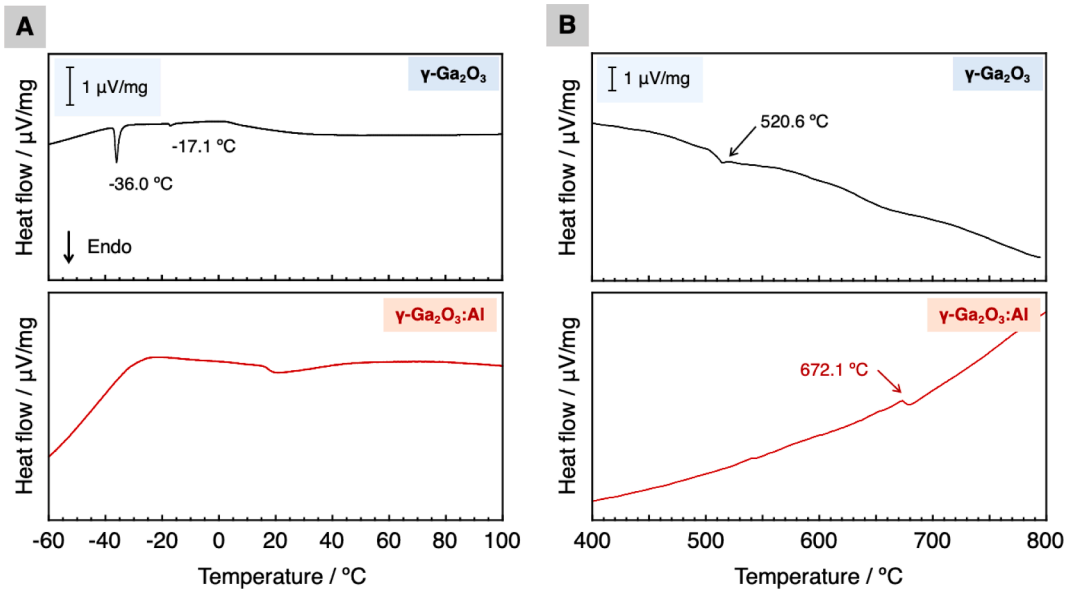

Fig. 10. DSC curve of γ-Ga_2O_3 and Al^{3+}-doped γ-Ga_2O_3 (A: range from −60 °C to 100 °C; B: range from 400 °C to 800 °C).

including microjet flow and shock waves [32] (first step of liquid Ga). However, because no dispersant was added to the reaction solution, Ga NPs were expected to fuse and be coarse due to interparticle collisions. Therefore, the Ga NPs underwent miniaturization and fusion again (second step of liquid Ga).

The redox potential of metallic Ga is −0.56 V_{SHE} [33], indicating that the surface of Ga NPs is easily oxidized by oxygen in the air. Herein, because ultrasound irradiation was conducted in the air, thin oxide films gradually formed on the surface of liquid Ga NPs over time (3rd step of liquid Ga). Such thin oxide films on liquid metal protect liquid metal particles from fusion and coarsening [10]; thus, the Ga NPs were stabilized by the thin oxide films. SEM revealed that the average diameter of Ga NPs after ultrasound miniaturization was 249 nm (Fig. 5).

4.1.2. *Ultrasound irradiation effect for Ga–Al liquid alloy*

In the case of the Ga–Al liquid alloy (lower part of Fig. 13), the Al-rich phase was segregated before ultrasonic treatment. This is because, according to the Ga–Al phase diagram, Ga–Al liquid alloy ([Ga^{3+}/Al^{3+} = 88:12 [atom%]) stabilizes at approximately 150 °C. Nevertheless, the XRD patterns (Fig. 4, right) show no crystalline peaks, indicating that the supersaturated Ga–Al alloy was stabilized as a liquid.

To understand the reason for the supersaturation, we investigated the synthetic methods for supersaturation states in other studies. Previous studies have shown that mechanical alloying, such as high-energy ball milling, is a synthetic method for supersaturated materials [24,34,35]. In mechanical alloying, to form and maintain supersaturated materials, a supersaturated state is formed by a localized high-temperature and -pressure field and maintained by quenching effects [35].

Ultrasonic processing also provides localized high-temperature and -pressure fields and quenching effects by rapid generation and extinction of hot spots in a span of microseconds. Therefore, supersaturated

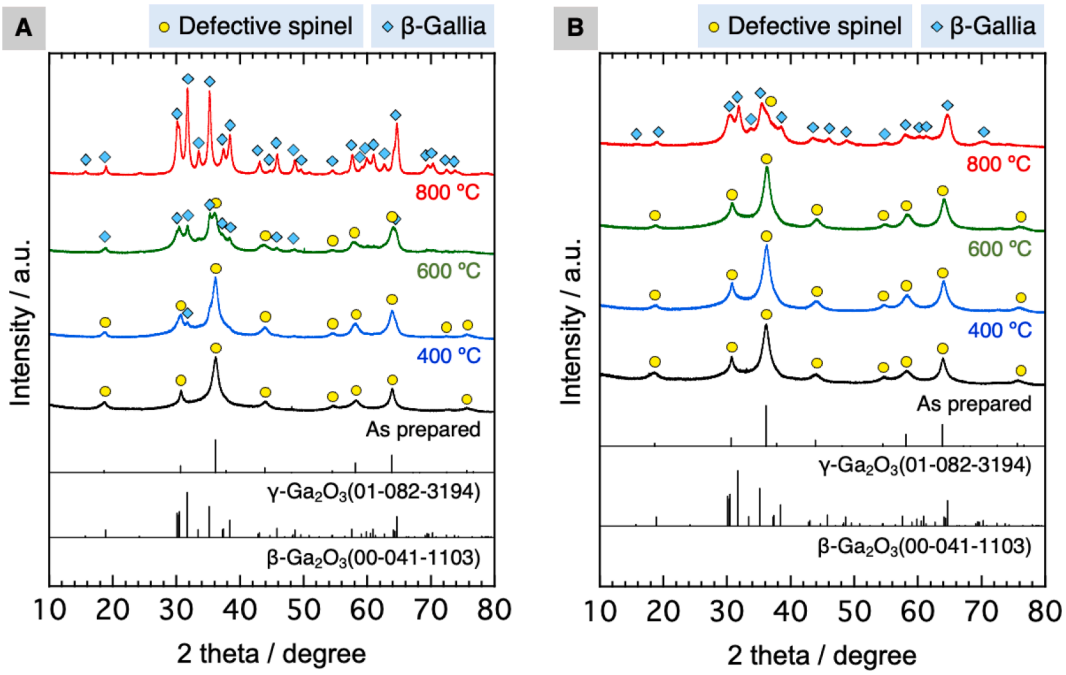

Fig. 11. XRD patterns of γ-Ga_2O_3 (A) and Al^{3+}-doped γ-Ga_2O_3 (B) calcined for 3 h at 400 °C–800 °C.

materials can be obtained by ultrasonic processing. When a Ga–Al alloy system is irradiated, the segregation parts dissolve in the Ga–Al liquid alloy due to the localized high-temperature and -pressure field of the hot spots (first step of Ga–Al liquid alloy). Because the rapid extinction of hot spots provides a quenching effect in a liquid alloy, a nonequilibrium reaction field is formed by ultrasonic irradiation, and the supersaturated state is maintained afterward. Therefore, the supersaturated Ga–Al liquid alloy ([Ga^{3+}/Al^{3+} = 88:12 [atom%]), which stabilizes at 150 °C, was obtained at 60 °C.

In the second step of Ga–Al liquid alloy formation, the supersaturated Ga–Al liquid alloy was miniaturized by shock waves and microjet flows, resulting in supersaturated Ga–Al fine particles. Considering the redox potentials of Ga (−0.56 V_{SHE}) and Al (−1.67 V_{SHE}) [33], the Ga–Al liquid alloy can be more basic than Ga and is easily oxidized. Thus, a thin oxide film was rapidly formed on the surface of Ga–Al liquid alloy particles (thrisd step of Ga–Al liquid alloy formation). The thin oxide film inhibited the miniaturization of the Ga–Al liquid alloy particles and promoted the stabilization of the alloy as microparticles before miniaturization progressed. Thus, the average diameter of the Ga–Al liquid alloy particles obtained after the ultrasonic irradiation was 1.72 μm, which is approximately-seven times higher than that of the Ga NPs (249 nm).

4.2. *Difference between the oxidation mechanisms of the Ga NPs and supersaturated Ga–Al particles*

4.2.1. *Effect of ultrasonic irradiation on the Ga NPs and the oxidation process*

Fig. 13 shows a schematic of the oxidation mechanism of liquid Ga (upper) and Ga–Al liquid alloy (lower). In the case of liquid Ga (upper part of Fig. 14), a small number of γ-Ga_2O_3 nuclei were slowly deposited on the surface of Ga NPs when the Ga surface was attacked by the oxygen species generated from the irradiated $N_2H_4{\cdot}H_2O$ in the first step of liquid Ga formation. After nucleation, the nuclei grew on the surface of Ga NPs, and γ-Ga_2O_3 crystals covered the Ga NPs. Thus, layers of γ-Ga_2O_3 crystals were formed on the surface of the Ga NPs, and γ-Ga_2O_3/liquid Ga core–shell particles were obtained. The layer of γ-Ga_2O_3 crystals inhibited the diffusion of active oxygen species and the oxidation of the core liquid Ga. For oxidation to proceed, the γ-Ga_2O_3 layer must crack so that the core Ga leaks. In this study, the γ-Ga_2O_3 layer cracked due to sonophysical effects (shock waves, micro-jet flows, intensive stirring, etc.). Liquid Ga, which leaked, was used for the grain growth of needle-shaped γ-Ga_2O_3 crystals on the surface. Thus, γ-Ga_2O_3 fine particles (D_{av} = 254 nm) with a hollow structure were obtained (third step of liquid Ga formation) after ultrasonic irradiation.

4.2.2. *Effect of ultrasonic irradiation on supersaturated Ga–Al particles and the oxidation process*

The oxidation mechanism of the Ga–Al liquid alloy was different from that of the liquid Ga, as shown in the lower part of Fig. 14. In the first step of Ga–Al liquid alloy formation, many oxide nuclei were rapidly formed when the surface of Ga–Al liquid alloy was attacked by oxygen species. This is because the redox potential of liquid Ga (−0.56 V_{SHE}) changes with Al-alloying (−1.67 V_{SHE}).

The redox potential of a metal can be adjusted by forming a solid solution with other metals [34,35]. Yang et al. reported that supersaturated Mg–Zn solid solution, synthesized by mechanical milling and laser sintering, has higher corrosion resistance than metallic Mg [35], which is attributed to the increase in the redox potential of Mg (−2.37 V_{SHE}) when Zn (−0.762 V_{SHE}) is introduced into the Mg matrix [33,35].

In the case of a Ga–Al liquid alloy, the redox potential of Ga (−0.56 V_{SHE}) decreases when it is alloyed with Al (−1.67 V_{SHE}). Thus, supersaturated Ga–Al liquid alloy is easily oxidized compared to liquid Ga. Therefore, many oxide nuclei were formed quickly during the oxidation of the supersaturated Ga–Al liquid alloy. In addition, ultrasonic effects (localized heating, intensive stirring, etc.) also promoted the oxidation reaction.

The XRD patterns of the liquid alloy (Fig. 12) show that Al^{3+} was doped into defect sites in the γ-Ga_2O_3 defective spinel structure during the oxidation of the Ga–Al liquid alloy. Considering the nonequilibrium field provided by ultrasound, Al^{3+} was introduced to defect sites by the localized high-temperature and -pressure fields and quenching effects of hot spots, which is difficult to achieve in general.

In the second step of the Ga–Al liquid alloy, the nuclei were easily detached from the surface of the liquid alloy due to sonophysical effects, such as shock waves, which resulted from the cavitation collapse. Consequently, Al^{3+}-doped γ-Ga_2O_3 nuclei could not grow during oxidation because the nuclei separated the liquid alloy, which is the raw

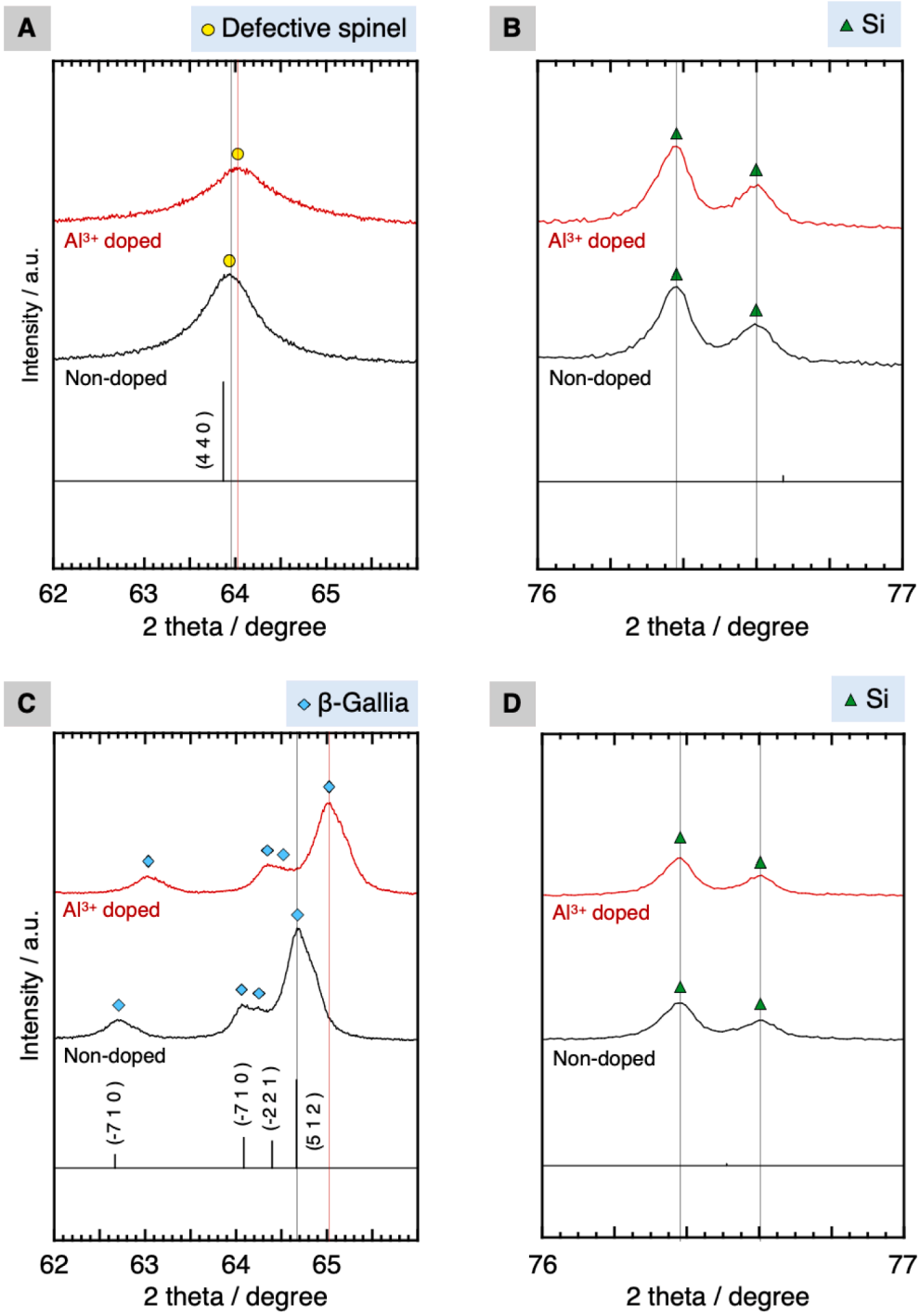

Fig. 12. XRD patterns of (A), (B) γ-Ga_2O_3 and Al^{3+}-doped γ-Ga_2O_3, (C), (D) β-Ga_2O_3 and Al^{3+}-doped β-Ga_2O_3. Silicon (Si) powder was added to each samples as internal standard. (A, C: peaks of γ- and β-Ga_2O_3; B, D: peaks of Si).

Table 1
Bandgaps of γ- and β-Ga_2O_3 calcined at different temperatures.

	Bandgap of γ-Ga_2O_3 [eV]	Bandgap of γ-Ga_2O_3:Al [eV]
Non-thermal treatment	4.91	5.17
Calcined at 400 °C	4.59	4.76
Calcined at 600 °C	4.46	4.75
Calcined at 800 °C	4.61	4.82

material for grain growth. This is because Al^{3+}-doped γ-Ga_2O_3 NPs were observed even at the early stage of the ultrasonic irradiation (1 h), as shown in Fig. 7. After the crystal nuclei were detached from the surface of the liquid alloy, and the metal surfaces were exposed, nucleation quickly reoccurred on the liquid alloy surface. The cycle of nucleation and detachment of nuclei was repeated until the Ga–Al liquid alloy was completely used for the nucleation (third step of Ga–Al liquid alloy formation). The Al^{3+}-doped γ-Ga_2O_3 NPs obtained after 24 h showed a high specific surface area (181 m^2/g) and an average diameter of 59 nm without dispersant.

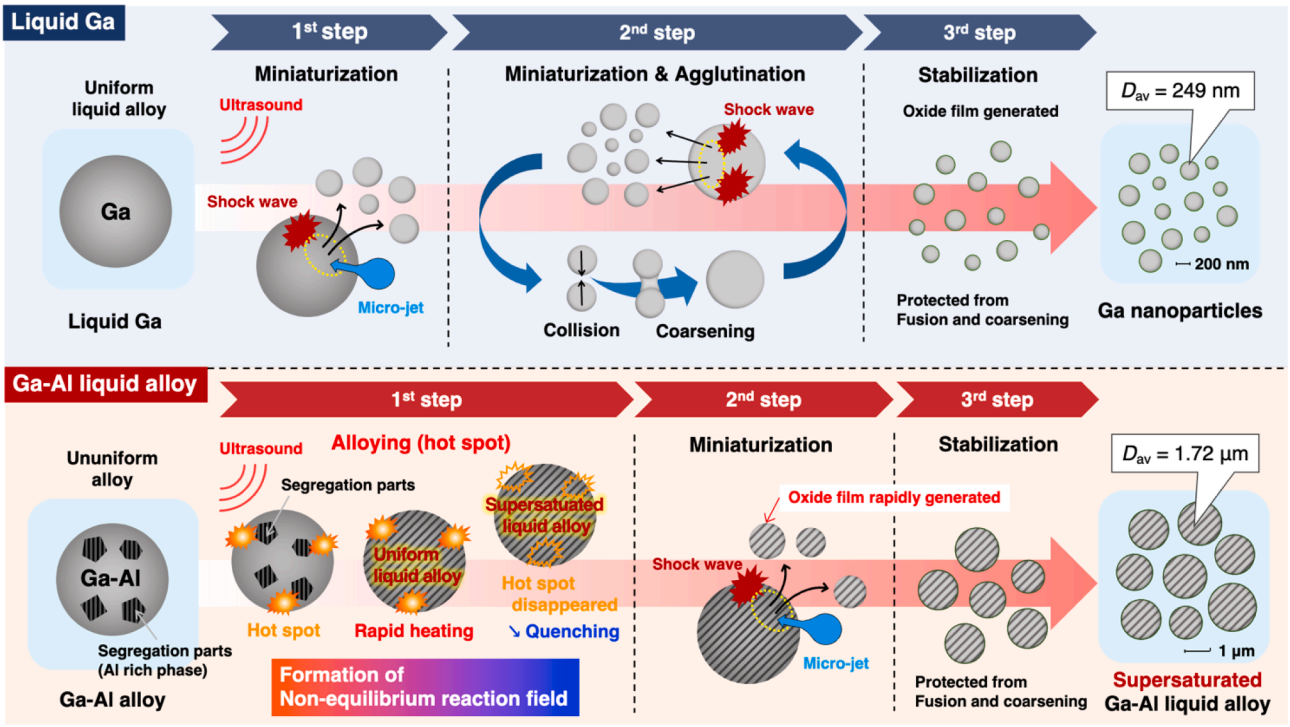

Fig. 13. Schematic of the miniaturization mechanism for liquid Ga and Ga–Al liquid alloy.

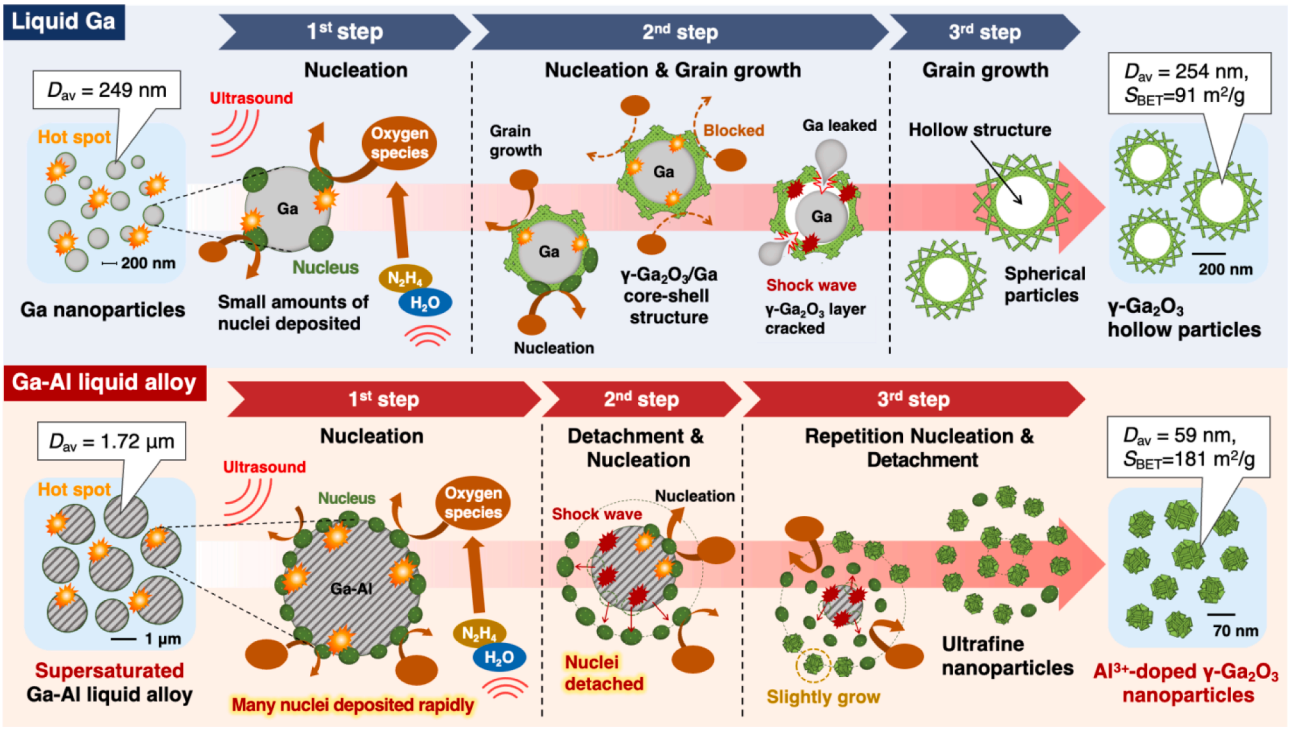

Fig. 14. Schematic of the oxidation mechanism of liquid Ga and Ga–Al liquid alloy.

5. Conclusions

In this study, we investigated the synthesis of supersaturated Ga–Al liquid alloy and Al^{3+}-doped γ-Ga_2O_3 NPs at near room temperature (60 °C) based on sonochemical and sonophysical effects via a two-step reaction (miniaturization and oxidation).

In the miniaturization step, high-temperature and -pressure field and quenching effects provided by ultrasound resulted in the formation of supersaturated Ga–Al liquid alloy. In the oxidation step, supersaturated Ga–Al liquid alloy was rapidly oxidized, and Al^{3+}-doped γ-Ga_2O_3 NPs were obtained after only 1-h irradiation at 60 °C. The Al^{3+}-doped γ-Ga_2O_3 NPs obtained after the ultrasonic processing showed a high specific surface area (S_{BET} = 181 m^2/g) and a small particle size (D_{av} = 59 nm). In this sonoprocessing, the supersaturated liquid alloy and

ceramic NPs were synthesized at near room temperature without a dispersant, thermal treatment, and the remain of counter anions, like $(NO_3)_3^-$, SO_4^{2-}, and Cl^-.

Materials with supersaturated compositions have been synthesized using thermodynamic nonequilibrium fields, as in mechanical alloying. Herein, we considered that ultrasonic processing also provides nonequilibrium reaction fields (localized high-temperature and -pressure effects, quenching effects, microjet flows, and shock waves) for material synthesis. Thus, based on these sonochemical and sonophysical effects, we explored sonochemical processing for synthesizing supersaturated materials.

Ceramics nanomaterials (oxides, nitrides, sulfides, etc.) have been synthesized via high-temperature heat treatment. In particular, γ-Ga_2O_3 NPs, which are a metastable phase of Ga_2O_3, are synthesized under harsh reaction conditions (high temperature, high pressure, low concentrations, long reaction time, etc.). However, herein, we achieved a high-yield synthesis of γ-Ga_2O_3-based NPs at near room temperature without a dispersant, thermal treatment, or leftover counter anions. Thus, sonochemical processing is an ecofriendly technique for synthesizing various supersaturated and ceramic nanomaterials and would promote the development of innovative sustainable development goals (SDGs)-oriented material processing techniques.

CRediT authorship contribution statement

Toshiki Yamanaka: Writing – original draft, Formal analysis. **Yamato Hayashi:** Conceptualization, Methodology, Investigation, Funding acquisition, Writing – review & editing, Project administration. **Hirotsugu Takizawa:** Supervision.

Declaration of Competing Interest

The authors declare that they have no known competing financial interests or personal relationships that could have appeared to influence the work reported in this paper.

Data availability

Data will be made available on request.

Acknowledgement

We would like to thank T. Kobayashi of Rasa Industries, Ltd for supplying of gallium metal.

References

[1] Z. Galazka, R. Uecker, D. Klimm, K. Irmscher, M. Naumann, M. Pietsch, A. Kwasniewski, R. Bertram, S. Ganschow, M. Bickermann, Scaling-up of bulk β-Ga_2O_3 single crystals by the czochralski method, ECS J. Solid State Sci. Technol. 6 (2017) Q3007–Q3011, https://doi.org/10.1149/2.0021702JSS/XML.

[2] N. Ueda, H. Hosono, R. Waseda, H. Kawazoe, Anisotropy of electrical and optical properties in β-Ga_2O_3 single crystals, Appl. Phys. Lett. 71 (1997) 933–935, https://doi.org/10.1063/1.119693.

[3] V.I. Nikolaev, V. Maslov, S.I. Stepanov, A.I. Pechnikov, V. Krymov, I.P. Nikitina, L. I. Guzilova, V.E. Bougrov, A.E. Romanov, Growth and characterization of β-Ga_2O_3 crystals, J. Cryst. Growth 457 (2017) 132–136, https://doi.org/10.1016/j.jcrysgro.2016.05.049.

[4] A. Kuramata, K. Koshi, S. Watanabe, Y. Yamaoka, T. Masui, S. Yamakoshi, High-quality β-Ga_2O_3 single crystals grown by edge-defined film-fed growth, Jpn. J. Appl. Phys. 55 (2016) 1202A2, https://doi.org/10.7567/JJAP.55.1202A2.

[5] M. Hirano, K. Sakoda, Y. Hirose, Direct formation and phase stability of luminescent γ-Ga_2O_3 spinel nanocrystals via hydrothermal method, J. Sol-Gel Sci. Technol. 77 (2016) 348–354, https://doi.org/10.1007/s10971-015-3860-8.

[6] H.Y. Playford, A.C. Hannon, M.G. Tucker, D.M. Dawson, S.E. Ashbrook, R. J. Kastiban, J. Sloan, R.I. Walton, Characterization of structural disorder in γ-Ga_2O_3, J. Phys. Chem. C 118 (2014) 16188–16198, https://doi.org/10.1021/jp5033806.

[7] C. Otero Areán, A.L. Bellan, M.P. Mentruit, M.R. Delgado, G.T. Palomino, Preparation and characterization of mesoporous γ-Ga_2O_3, Microporous Mesoporous Mater. 40 (1-3) (2000) 35–42.

[8] Y. Hayashi, H. Takizawa, M. Inoue, K. Niihara, K. Suganuma, Ecodesigns and applications for noble metal nanoparticles by ultrasound process, IEEE Trans. Electron. Packag. Manuf. 28 (2005) 338–343, https://doi.org/10.1109/TEPM.2005.858452.

[9] Y. Maeda, Y. Hayashi, J. Fukushima, H. Takizawa, Sonochemical effect and pore structure tuning of silica xerogel by ultrasonic irradiation of semi-solid hydrogel, Ultrason. Sonochem. 73 (2021) 105476, https://doi.org/10.1016/j.ultsonch.2021.105476.

[10] H. Friedman, S. Reich, R. Popovitz-Biro, P. von Huth, I. Halevy, Y. Koltypin, A. Gedanken, Z. Porat, Micro- and nano-spheres of low melting point metals and alloys, formed by ultrasonic cavitation, Ultrason. Sonochem. 20 (2013) 432–444, https://doi.org/10.1016/j.ultsonch.2012.08.009.

[11] H. Friedman, Z. Porat, I. Halevy, S. Reich, Formation of metal microspheres by ultrasonic cavitation, J. Mater. Res. 25 (2010) 633–636, https://doi.org/10.1557/JMR.2010.0083.

[12] N. Wang, L. Zhu, D. Wang, M. Wang, Z. Lin, H. Tang, Sono-assisted preparation of highly-efficient peroxidase-like Fe_3O_4 magnetic nanoparticles for catalytic removal of organic pollutants with H_2O_2, Ultrason. Sonochem. 17 (2010) 526–533, https://doi.org/10.1016/j.ultsonch.2009.11.001.

[13] S. Avivi, Y. Mastai, G. Hodes, A. Gedanken, Sonochemical hydrolysis of Ga^{3+} ions: Synthesis of scroll-like cylindrical nanoparticles of gallium oxide hydroxide, J. Am. Chem. Soc. 121 (1999) 4196–4199, https://doi.org/10.1021/ja9835584.

[14] H. Ataee-Esfahani, L. Wang, Y. Nemoto, Y. Yamauchi, Synthesis of bimetallic Au@Pt nanoparticles with Au core and nanostructured Pt shell toward highly active electrocatalysts, Chem. Mater. 22 (2010) 6310–6318, https://doi.org/10.1021/cm102074w.

[15] J.R. BlakePerutz, K.S. Suslick, Y. Didenko, M.M. Fang, T. Hyeon, K.J. Kolbeck, W. B. McNamara, M.M. Mdleleni, M. Wong, Acoustic cavitation and its chemical consequences, Philos. Trans. R. Soc. London. Series A: Math. Phys. Eng. Sci. 357 (1751) (1999) 335–353, https://doi.org/10.1098/RSTA.1999.0330.

[16] V.B. Kumar, A. Gedanken, G. Kimmel, Z. Porat, Ultrasonic cavitation of molten gallium: Formation of micro- and nano-spheres, Ultrason. Sonochem. 21 (2014) 1166–1173, https://doi.org/10.1016/j.ultsonch.2013.11.004.

[17] V.B. Kumar, A. Gedanken, Z. Porat, Facile synthesis of gallium oxide hydroxide by ultrasonic irradiation of molten gallium in water, Ultrason. Sonochem. 26 (2015) 340–344, https://doi.org/10.1016/j.ultsonch.2015.03.012.

[18] R. Tokura, H. Tsukamoto, T. Tokunaga, M.T. Nguyen, T. Yonezawa, The role of surface oxides and stabilising carboxylic acids of copper nanoparticles during low-temperature sintering, Materials, Advances. 3 (2022) 4802–4812, https://doi.org/10.1039/D1MA01242H.

[19] T. Yonezawa, Y. Uchida, H. Tsukamoto, X-ray diffraction and high-resolution TEM observations of biopolymer nanoskin-covered metallic copper fine particles: preparative conditions and surface oxidation states, Phys. Chem. Chem. Phys. 17 (2015) 32511–32516, https://doi.org/10.1039/C5CP06107E.

[20] Y. Takano, Y. Hayashi, J. Fukushima, H. Takizawa, Room-temperature synthesis of γ-Ga_2O_3 nanoparticles from gallium metal via ultrasound irradiation, Adv. Powder Technol. 32 (2021) 860–865, https://doi.org/10.1016/j.apt.2021.01.032.

[21] M. Ghasemi, J. Johansson, Thermodynamic assessment of the As-Zn and As-Ga-Zn systems, J. Alloy. Compd. 638 (2015) 95–102, https://doi.org/10.1016/j.jallcom.2015.03.051.

[22] S. Kulawik, W. Gierlotka, A. Dębski, W. Gąsior, A. Zajączkowski, Calorimetric and phase diagram studies of the Ga-In-Zn system, J. Mol. Liq. 325 (2021) 115114, https://doi.org/10.1016/J.MOLLIQ.2020.115114.

[23] A. Dobosz, T. Gancarz, Density, viscosity and surface tension of gallium rich Al-Ga alloys, Fluid Phase Equilib. 532 (2021) 112923, https://doi.org/10.1016/J.FLUID.2020.112923.

[24] A. Suda, T. Kandori, N. Terao, Y. Ukyo, H. Sobukawa, M. Sugiura, Formation of CeO_2-ZrO_2 solid solution during attrition milling of CeO_2 powder, J. Mater. Sci. Lett. 17 (1998) 89–90, https://doi.org/10.1023/A:1006514329090.

[25] S. Romankov, S.D. Kaloshkin, Y. Hayasaka, N. Hayashi, E. Kasai, S.v. Komarov, Effect of process parameters on the formation of Ti-Al coatings fabricated by mechanical milling, J. Alloy. Compd. 484 (2009) 665–673, https://doi.org/10.1016/j.jallcom.2009.05.016.

[26] T. Oshima, Y. Kato, M. Oda, T. Hitora, M. Kasu, Epitaxial growth of γ-$(Al_xGa_{1-x})O_3$ alloy films for band-gap engineering, Appl. Phys Express 10 (2017) 051104, https://doi.org/10.7567/APEX.10.051104.

[27] J. Mingear, Z. Farrell, D. Hartl, C. Tabor, Gallium–indium nanoparticles as phase change material additives for tunable thermal fluids, Nanoscale 13 (2021) 730–738, https://doi.org/10.1039/D0NR06526A.

[28] M. Takahashi, T. Nakatani, S. Iwamoto, T. Watanabe, M. Inoue, Effect of modification by alkali on the γ-Ga_2O_3-Al_2O_3 mixed oxides prepared by the solvothermal method, J. Phys.: Condens. Matter 18 (2006) 5745–5757, https://doi.org/10.1088/0953-8984/18/24/015.

[29] M. Takahashi, N. Inoue, T. Takeguchi, S. Iwamoto, M. Inoue, T. Watanabe, Synthesis of γ-Ga_2O_3-Al_2O_3 solid solutions by the glycothermal method, J. Am. Ceram. Soc. 89 (2006) 2158–2166, https://doi.org/10.1111/j.1551-2916.2006.01060.x.

[30] H.Y. Playford, A.C. Hannon, E.R. Barney, R.I. Walton, Structures of uncharacterised polymorphs of gallium oxide from total neutron diffraction, Chem. Eur. J. 19 (2013) 2803–2813, https://doi.org/10.1002/CHEM.201203359.

[31] R.D. Shannon, Revised effective ionic radii and systematic studies of interatomie distances in halides and chaleogenides, Acta Cryst. 32 (1976) 751.

[32] T. Yamamoto, R. Matsutaka, S.v. Komarov, High-speed imaging of ultrasonic emulsification using a water-gallium system, Ultrason. Sonochem. 71 (2021) 105387, https://doi.org/10.1016/J.ULTSONCH.2020.105387.

[33] B.S.C.Jr. Stephen D. Cramer, Electrochemical Series, Corrosion: Materials. 13B (2005) 665–671. 10.31399/ASM.HB.V13B.A0006542.
[34] C. Shuai, C. He, G. Qian, A. Min, Y. Deng, W. Yang, X. Zang, Mechanically driving supersaturated Fe–Mg solid solution for bone implant: Preparation, solubility and degradation, Compos. B Eng. 207 (2021) 108564, https://doi.org/10.1016/J.COMPOSITESB.2020.108564.
[35] Y. Yang, W. Wang, M. Yang, Y. Yang, D. Wang, Z. Liu, C. Shuai, Laser-sintered Mg-Zn supersaturated solid solution with high corrosion resistance, Micromachines 12 (2021) 1368, https://doi.org/10.3390/MI12111368.